Eur J Nucl Med Mol Imaging (2018) 45:355–364
https://doi.org/10.1007/s00259-017-3875-1

ORIGINAL ARTICLE

Prospective evaluation of ^{18}F-FACBC PET/CT and PET/MRI versus multiparametric MRI in intermediate- to high-risk prostate cancer patients (FLUCIPRO trial)

Ivan Jambor[1,2,3] · Anna Kuisma[4] · Esa Kähkönen[5] · Jukka Kemppainen[3,6] · Harri Merisaari[1,3,7] · Olli Eskola[3] · Jarmo Teuho[3] · Ileana Montoya Perez[1,7,8] · Marko Pesola[1] · Hannu J. Aronen[1,8] · Peter J. Boström[5] · Pekka Taimen[9] · Heikki Minn[3,4]

Received: 15 July 2017 / Accepted: 3 November 2017 / Published online: 16 November 2017

Abstract
Purpose The purpose of this study was to evaluate ^{18}F-FACBC PET/CT, PET/MRI, and multiparametric MRI (mpMRI) in detection of primary prostate cancer (PCa).
Methods Twenty-six men with histologically confirmed PCa underwent PET/CT immediately after injection of 369 ± 10 MBq ^{18}F-FACBC (fluciclovine) followed by PET/MRI started 55 ± 7 min from injection. Maximum standardized uptake values (SUV_{max}) were measured for both hybrid PET acquisitions. A separate mpMRI was acquired within a week of the PET scans. Logan plots were used to calculate volume of distribution (V_T). The presence of PCa was estimated in 12 regions with radical prostatectomy findings as ground truth. For each imaging modality, area under the curve (AUC) for detection of PCa was determined to predict diagnostic performance. The clinical trial registration number is NCT02002455.
Results In the visual analysis, 164/312 (53%) regions contained PCa, and 41 tumor foci were identified. PET/CT demonstrated the highest sensitivity at 87% while its specificity was low at 56%. The AUC of both PET/MRI and mpMRI significantly ($p < 0.01$) outperformed that of PET/CT while no differences were detected between PET/MRI and mpMRI. SUV_{max} and V_T of Gleason score (GS) >3 + 4 tumors were significantly ($p < 0.05$) higher than those for GS 3 + 3 and benign hyperplasia. A total of 442 lymph nodes were evaluable for staging, and PET/CT and PET/MRI demonstrated true-positive findings in only 1/7 patients with metastatic lymph nodes.
Conclusions Quantitative ^{18}F-FACBC imaging significantly correlated with GS but failed to outperform MRI in lesion detection. ^{18}F-FACBC may assist in targeted biopsies in the setting of hybrid imaging with MRI.

Keywords ^{18}F-FACBC · Prostate cancer · Diffusion-weighted imaging · PET/CT · PET/MRI

Ivan Jambor and Anna Kuisma have contributed equally to this work

Electronic supplementary material The online version of this article (https://doi.org/10.1007/s00259-017-3875-1) contains supplementary material, which is available to authorized users.

✉ Ivan Jambor
ivan.jambor@utu.fi

[1] Department of Diagnostic Radiology, University of Turku, Kiinamyllynkatu 4-8, P.O. Box 52, FI-20521 Turku, Finland

[2] Department of Radiology, University of Massachusetts Medical School – Baystate, Springfield, MA, USA

[3] Turku PET Centre, Turku, Finland

[4] Department of Oncology and Radiotherapy, Turku University Hospital, Turku, Finland

[5] Department of Urology, Turku University Hospital, Turku, Finland

[6] Department of Clinical Physiology and Nuclear Medicine, Turku University Hospital, Turku, Finland

[7] Department of Information Technology, University of Turku, Turku, Finland

[8] Medical Imaging Centre of Southwest Finland, Turku University Hospital, Turku, Finland

[9] Department of Pathology, University of Turku and Turku University Hospital, Turku, Finland

Introduction

Prostate cancer (PCa) remains the second most common cause of cancer-related death in the western world [1]. Despite encouraging results with multiparametric magnetic resonance imaging (mpMRI), more advanced techniques enabling accurate PCa detection may offer additional benefit. Routine mpMRI of the prostate is still limited by its poor specificity to differentiate "significant" from "indolent" PCa [2]. Development and validation of novel methods for non-invasive detection of prostate cancer aggressiveness could enable improved risk stratification. Such approaches would ideally offer high repeatability/reproducibility, good diagnostic performance, and rapid imaging acquisition while being patient friendly. Gleason score (GS), tumor stage and prostate-specific antigen (PSA) are parts of clinical nomograms used in treatment decision planning in an attempt to improve characterization of PCa [3]. Unfortunately, GS from systematic TRUS-guided biopsy is commonly lower than "true" GS from prostatectomy [4].

Although positron emission tomography/computerized tomography (PET/CT) with ^{18}F-Fluorodeoxyglucose (FDG) is widely used in oncology, it is rarely applied to evaluate patients with localized PCa. Tracers depicting lipid metabolism such as ^{11}C–acetate [5, 6], or ^{11}C/^{18}F–choline [7], which is a tracer incorporated into lipids, are applicable for detection of biochemical recurrence but have not demonstrated sufficiently high specificity to justify routine imaging of organ-confined disease [8]. Many cancers, including PCa, have upregulated amino acid transport linked to their proliferative potential [9, 10]. The synthetic non-metabolized leucine derivate anti-1-amino-3-^{18}F-fluorocyclobutane-1-carboxylic acid (^{18}F-FACBC) accumulates in PCa [11] and may offer better diagnostic potential than ^{11}C–choline in patients presenting with biochemical recurrence [12]; however, in parallel with lipid tracers, ^{18}F-FACBC accumulates both in PCa and benign prostatic hyperplasia (BPH) [13]. A combination of functional and anatomical information with hybrid imaging could overcome this problem; therefore, we compared ^{18}F-FACBC PET/CT, PET/MRI, and mpMRI in detection and characterization of PCa in patients undergoing robot-assisted radical prostatectomy, focusing on the potential to detect intraprostatic disease and pelvic lymph nodes.

Material and methods

Patients

Between January 2014 and June 2015, a total of 32 men with histologically confirmed PCa scheduled for radical robot-assisted prostatectomy were prospectively enrolled (median age, 65 years; range, 49–76). The median serum PSA was 12.0 (range, 4.1–35) ng/ml. Six men could not have all scans for logistical reasons or refusal to participate after signing approved informed consent. Thus, 26 patients underwent ^{18}F-FACBC PET/CT followed by ^{18}F-FACBC PET/MRI performed in succession and a separate mpMRI within a median 12 (range, 1–119) days. The clinical trial registration number is NCT02002455 (www.clinicaltrials.gov). All anonymized ^{18}F-FACBC PET/CT, PET/MRI, mpMRI data sets, scanned whole mount prostatectomy sections, and mpMRI reports are freely available (NOTE: to be made freely available following publication) at the following address: http://petiv.utu.fi/flucipro. (NOTE: the user accounts for reviewers and editors are as follows- user name: flucipro, password: flucipropassword).

Synthesis of ^{18}F-FACBC

^{18}F-FACBC (fluciclovine) synthesis was performed by using a FASTlab™ Synthesizer (GE Healthcare, Waukesha, WI, USA) as the production module and the FASTlab cassettes (GE Healthcare) and synthesis sequence designed for ^{18}F-FACBC production.

^{18}F-FACBC PET/CT

^{18}F-FACBC PET/CT imaging data were acquired using a hybrid Discovery 690 PET/CT scanner (General Electric Medical Systems, Milwaukee, WI, USA) with a 64-slice CT and PET operated in three-dimensional mode, with an in-plane PET full-width at half-maximum of 4 mm [14]. All quantitative corrections applied to the PET sinogram data took into account detector dead time, radioactivity decay, random scatter, and photon attenuation. PET images were reconstructed in a 128 × 128 matrix with a voxel size of 5.47 × 5.47 × 3.27 mm^3, using the VUE Point FX algorithm with time-of-flight technology and a 6-mm Gaussian post-filter and no resolution modeling.

Before imaging, each patient was asked to fast for 4–6 h and empty the rectum, but no enema was used. Each participant received an intravenous injection of 369 ± 10 MBq (mean ± standard deviation) of ^{18}F-FACBC diluted in 3–5 ml of saline as a 30-s bolus that was promptly flushed with saline. Emission imaging with the prostate in the center of the field of view was started immediately after the injection, preceded by pre-injection transmission imaging using low-dose CT. Following 20 min of dynamic data collection with a list-mode acquisition, additional table positions covering the whole pelvis and abdomen were acquired with 4-min durations per position. The dynamic data were reconstructed to five frames with a frame time of 4 min.

^{18}F-FACBC PET/MRI

Following PET/CT imaging, patients were transferred to the PET/MRI suite housing the Ingenuity TF PET/MRI scanner (Phillips Medical Systems, Cleveland, OH). MR-based attenuation correction was performed as described previously [15]. All quantitative corrections were made to the PET data, taking into account detector dead time, radioactivity decay, random scatter, and photon attenuation. PET images were reconstructed in a 144 × 144 matrix with an isotropic voxel size of 4 mm. PET/MRI studies were started with the attenuation correction in the MRI gantry, followed by a move to the PET gantry for PET imaging. Two table positions of 4 min each covering the whole pelvis were acquired. Finally, the patient table was moved back to the MRI gantry for acquiring MRI data. T2-weighted (T2w) images were obtained using a single-shot turbo spin-echo sequence followed by diffusion-weighted imaging (DWI) with a single-shot spin-echo-based sequence with a monopolar diffusion gradient scheme and echo-planar readout. DWI was performed as previously described using 12 b values (0, 100, 300, 500, 700, 900, 1100, 1300, 1500, 1700, 1900, 2000) [16–20]. Finally, T2w and DWI (performed using b values of 0 and 800 s/mm^2) covering the whole pelvis were obtained. Additional MR acquisitions were acquired [16, 21] but not evaluated in the current study.

Multiparametric MRI

mpMRI was performed using a 3-T MR scanner (Magnetom Verio 3 T, Siemens Healthcare, Erlangen, Germany) and surface array coils as previously described [22]. The imaging consisted of triplanar T2w turbo spin-echo imaging, single-shot spin-echo-based DWI, and DCE-MRI. Two separate single-shot spin-echo-based DWI acquisitions were performed [22, 23] using 5 b values (0, 100, 200, 350, 500 s/mm^2) and 16 b values (0, 50, 100, 200, 350, 500, 650, 800, 950, 1100, 1250, 1400, 1550, 1700, 1850, 2000 s/mm^2) [24]. Additional MR acquisitions such as three-dimensional ^{1}H–MRS were done but were not evaluated in the current study.

Visual evaluation

An experienced nuclear medicine physician (JK), with 10 years of experience in prostate PET/CT at the beginning of the trial, and a PhD student (IJ), with 3 years of experience in prostate PET/CT at the beginning of the trial, interpreted the PET/CT images, aware of the PCa diagnosis but not of other clinical and histopathological findings. A previously described region-based approach was used in visual evaluation of PET/CT [25], leading to estimates of PCa presence in 12 regions. Abnormal uptake was defined as any mono- or multifocal uptake greater than adjacent background in >1 slice within the CT-defined prostate gland area [26].

mpMRI was scored using a Likert system [22, 27] by a PhD student (IJ) with 4 years of experience in prostate mpMRI at the beginning of the trial and more than 250 previous cases reported where pathologic confirmation at surgery was available. Following trial completion, PI-RADs version 2 scores were added to the reports. mpMRI reporting was done in an anonymized random fashion blinded to PET/CT or PET/MR data sets.

The same readers visually evaluated PET/MRI in consensus using the same region-based analysis [25], visualizing T2w, DWI (trace and parametric maps), and PET images simultaneously. Any mono- or multifocal uptake of ^{18}F-FACBC originating from nodules of BPH identified on T2w and DWI was not considered to represent PCa. Focal uptake in the central gland and peripheral zone beyond that of adjacent background with no pathological changes on T2w and DWI or related to benign conditions was considered to be a tumor focus [26].

Quantitative evaluation

Logan plots [28] with a reference region in the iliac/femoral artery were used to estimate the tracer distribution volume (V_T) based on the assumption that transport of ^{18}F-FACBC into cells is similar to reversible receptor binding kinetics [13]. DWI datasets were post-processed at a voxel level using monoexponential function (apparent diffusion coefficient - ADC).

Histopathologic analysis

Whole-mount prostatectomy sections were prepared as described [19] and analyzed together by an experienced genitourinary pathologist (PT). Whole-mount axial macrosections were obtained at 5-mm (range 4–6) intervals in plane perpendicular to the long axis of the prostate gland in a superior–inferior direction. The most apical and basal macrosections were further sectioned in coronal orientation for better evaluation of the capsular status at the inferior and superior regions. Subsequently, the tissues were embedded in paraffin using macro-cassettes and the histological sections were cut at 4 micrometers and stained with hematoxylin and eosin. The presence and location of cancer foci, high-grade prostatic intraepithelial neoplasia, prostatitis, BPH, capsular status, and seminal vesicle invasion were determined. For each tumor focus, GS was assigned as a combination of primary, secondary, and tertiary (when applicable) Gleason grade [29]. Tertiary Gleason grade was assigned only if a Gleason grade pattern higher than the primary and secondary grades was present and the tertiary grade component was estimated visually to represent less than 5% of the tumor [30]. Tumors were classified into three groups: GS 3 + 3, 3 + 4, and >3 + 4. Only tumor foci >0.5 cm, largest

lesion diameter, as defined using whole-mount prostatectomy sections, were included in analyses.

Statistical analysis

Normally distributed continuous variables are given as means and standard deviations, variables not following normality as medians and interquartile ranges, and categorical variables as frequencies and proportions. The Kolmogorov–Smirnov test was used to check normality. ANOVA with the Bonferroni test or Kruskal–Wallis test with Dunn's test were used to compare parameter values for different tissue/cancer types, when appropriate. Two-sided p values were calculated. Diagnostic accuracy values [sensitivity, specificity, accuracy, area under the curve (AUC)] on the region level (n = 12) were calculated. Sensitivity and specificity values were compared using the McNemar test, and two-sided p values were calculated. Receiver operating characteristic curve analysis using 100,000 bootstrap samples [31], accounting for within-patient correlations, was used to estimate AUC values, which were compared as previously described [32]; 95% confidence intervals (CIs) for AUC values also were calculated using 100,000 bootstrap samples. A $p < 0.05$ was considered statistically significant. Statistical analyses were performed using MATLAB (Mathworks Inc., Natick, MA, USA) and/or GraphPad Prism, version 5.00 (GraphPad Software, San Diego, CA, USA). Post-processing codes as well as all MR sequences are freely available upon request.

Results

Imaging and surgical procedure

Twenty-six patients underwent ^{18}F-FACBC PET/CT followed by PET/MRI with a median time of 54 (range, 32–82) min between tracer injection and mid-frame time of PET/MRI. No adverse events were associated with ^{18}F-FACBC injections, and all patients tolerated the imaging procedure well.

Robot-assisted radical prostatectomy was performed within a median of 11 (range, 0–27) days after the hybrid PET studies; clinical and surgical findings are summarized in Table 1. Among whole-mount prostatectomy samples, 51 tumor foci were identified in 26 patients; 41 (80%) were >0.5 cm, of which 8, 13, and 20 represented GS 3 + 3, 3 + 4, and >3 + 4, respectively. Positive surgical margins were detected in 8 (8/26, 30%) and seminal vesicle invasion in 9 (9/26, 35%) patients. At lymphadenectomy, a median of 16 (range, 8–36; total = 446) nodes were removed; metastatic involvement was found in 23 nodes of 7 (27%) patients. Residual cancer based on PSA >0.2 ng/ml at 3 months after prostatectomy was seen in two patients; original imaging for one of these patients was already suspicious for metastatic disease (Fig. 1).

Diagnostic accuracy in region-based analysis

In the region-based analysis, 164/312 (53%) regions contained PCa based on the whole-mount prostatectomy sections. Among the three modalities studied, ^{18}F-FACBC PET/CT demonstrated the highest sensitivity (87%) and lowest specificity (56%; $p < 0.001$), with AUC = 0.72 (95%CI 0.65–0.80; $p < 0.001$). Sensitivity and specificity were 84% and 96% for PET/MRI and 77% ($p < 0.01$) and 99% for mpMRI, respectively, with AUC values of 0.90 (0.86–0.94) and 0.88 (0.83–0.93), respectively. p values are two-sided and compared to the highest values for each measure (Table 2).

Typically, index lesions were well depicted on ^{18}F-FACBC PET/CT and other modalities (Figs. 2, 3 and Supporting material Figs. S1, S2, S3, S4, S5). ^{18}F-FACBC PET/MRI led to significantly ($p < 0.001$) improved specificity of 96% by clearly decreasing false-positive findings associated with tracer uptake in BPH (Supporting material Fig. S6 and S7). BPH in turn was well classified by MRI-based modalities; only one region was false positive in mpMRI readings, resulting in a 96% specificity. ^{18}F-FACBC PET/MRI resulted in mildly improved sensitivity compared with mpMRI (Supporting material Fig. S7). Both ^{18}F-FACBC PET/MRI and mpMRI outperformed ^{18}F-FACBC PET/CT ($p < 0.01$) in AUC analysis, but diagnostic accuracy did not differ between ^{18}F-FACBC PET/MRI and mpMRI. All identified lesions on mpMRI were scored as 5 (highly suspicious; Likert) or 4–5 (PI-RADs version 2.0).

Staging accuracy

Exact agreement between preoperative stage based on all three imaging modalities and pathological stage was seen in 12 (46%) patients (Table 1). In general, no differences were detected between mpMRI and the MRI contribution of PET/MRI for T stage prediction; imaging correctly predicted the stage for less than half of the cases. In 11 (42%) patients, focal, 1–2-mm extra-capsular extension (stage T3a) was not identified. In three of nine patients (33%), seminal vesicle invasion (stage T3b) was correctly detected; a suspicion of invasion was present in two other patients on PET/MRI and mpMRI, but the related prostatectomy specimens were not positive for invasion.

Sensitivity was poor for detection of pelvic lymph node metastases for both ^{18}F-FACBC PET/CT and PET/MR, with no differences between DWI and PET. Hybrid PET modalities identified histologically confirmed lymph node metastases in only one of seven patients (17%). This patient (no. 20) had 13/22 metastatic lymph nodes and showed PET-positive left upper ramus and sacral metastases not visible on CT or scintigraphy. The size of metastatic lymph nodes not identified in the remaining six patients was <8 mm.

Table 1 Patient characteristics

Running no.	PSA [ng/ml]	Gleason score at biopsy	Flucipro TNM stage*	Flucipro risk group†	Pathological TNM	Postop risk group†	Surgical margins [mm]	Prostatectomy Gleason score	Lymph nodes		Size of PET +ve nodes [mm]	3-month PSA [ng/ml]
									Removed	Metastatic		
1	4.3	4 + 3	T2cN0	3	T2cN0	3	0	4 + 3 + 5	10	0	NA	0.003
2	4.1	4 + 3	T2aN0	3	T3aN0	3	0	3 + 4	11	0	NA	0.007
3	4.6	3 + 4	T2cN0	3	T3aN0	3	0	4 + 4	10	0	NA	0.003
4	8.1	4 + 3	T2cN0	3	T3aN0	3	0	4 + 3	31	0	NA	0.14
5	8.9	4 + 5	T3aN0	3	T3bN1	4	0	4 + 3	10	1	5	0.27
6	7.2	3 + 4	T2aN0	2	T2aN0	2	0	3 + 4	10	0	NA	0.003
7	7.6	4 + 3	T3aN0	3	T3aN0	3	3	4 + 3	16	0	NA	0.019
8	12	4 + 5	T2cN0	3	T2aN0	3	0	4 + 5	8	0	NA	0.091
9	8.3	4 + 3	T2cN0	3	T3aN0	3	0	4 + 3	8	0	NA	0.003
10	35	3 + 4	T3bN0	4	T3aN0	3	4	3 + 4	17	0	NA	0.024
11	6.2	4 + 3	T2cN0	3	T2cN0	3	0	3 + 4 + 5	10	0	NA	0.003
12	24	4 + 3	T3bN0	4	T3bN0	4	1	4 + 3	29	0	NA	0.005
13	16	4 + 5	T3bN0	4	T3bN0	4	6	4 + 5	21	0	NA	0.003
14	11	4 + 4	T2cN0	3	T3bN1	4	0	3 + 4	8	1	4.5	0.037
15	16	3 + 4	T2cN0	3	T3bN1	4	0	4 + 3	22	3	2–7	0.033
16	6.5	4 + 3	T2bN0	3	T3bN0	4	2	4 + 3 + 5	29	0	NA	0.005
17	7.7	3 + 4	T2cN0	3	T3aN0	3	5	3 + 4	12	0	NA	0.05
18	13	3 + 4	T2cN0	3	T3aN0	3	0	3 + 4	25	0	NA	0.003
19	18	3 + 4	T2aN0	3	T3aN1	4	0	3 + 4	7	1	1	0.003
20	26	5 + 4	T3bN1M1	4	T3bN1M1	4	50	5 + 4	22	13	1–25	5.4
21	5.3	3 + 4	T2cN0	3	T3aN0	3	0	3 + 4	26	0	NA	0.003
22	7.6	5 + 3	T3aN0	3	T3bN1	4	10	5 + 4	16	1	2	0.032
23	21	3 + 3	T2cN0	3	T2cN0	3	11	3 + 4	16	0	NA	0.003
24	14	4 + 5	T3bN0	4	T3bN0	4	0	4 + 5	13	0	NA	0.003
25	6.7	4 + 5	T3aN0	3	T3bN1	4	0	4 + 5	36	3	1.5–4.5	0.1
26	14.7	3 + 4	T3aN0	3	T2aN0	3	0	4 + 3	23	0	NA	0.026

*Flucipro stage based on all study imaging findings

† Low: 1; intermediate: 2; high: 3; very high: 4; T stage was based on the MRI part of PET/MRI and/or mpMRI while N stage was based on PET and DWI of PET/MRI (1)

NA = not applicable

Quantitative analysis of ^{18}F-FACBC PET

Median time activity curves (Fig. 4) indicate early uptake of tracers in a tumor and BPH and gradual washout that degraded the specific signal towards the end of the acquisition time. As tumor-to-BPH and tumor-to-normal prostate ratios showed, however, early imaging did not assist in discriminating cancer from BPH based on metabolic activity. The median SUV_{max} of 41 cancerous lesions at 12–22 min was 4.3 (range, 1.1–16.2), while it was 3.2 (range, 1.3–4.2) in 22 BPH nodules and 2.9 (range 1.1–3.9) in normal prostate. Nevertheless, the SUV_{max} difference between cancer ($n = 41$) and normal prostate ($n = 22$) was significant ($p < 0.001$), as was that between cancer and BPH ($p < 0.05$; Fig. 5), largely because of the higher SUV_{max} of GS >3 + 4 tumors ($n = 20$) compared to GS 3 + 4 and 3 + 3 tumors ($p < 0.05$); when SUV_{max} values of GS 3 + 4 and 3 + 3 tumors only were compared to BPH, differences were not significant.

The late acquisition of PET/MRI at a median of 54 (range, 32–82) min after injection clearly reduced the specific signal compared to BPH or normal prostate. The median SUV_{max} of 2.1 (range, 0.8–5.5) for 41 tumors on PET/MRI did not differ significantly from that for BPH (1.7; range, 0.63–2.1) or normal prostate (1.6; range, 0.58–2.1).

Logan plots became linear after the first time point (4 min). PCa and normal prostate differed significantly for V_T, but PCa and BPH did not. The median V_T for tumors was 2.6 (range, 1.1–8.9); values were 2.4 (range, 1.4–3.2) and 2.1 (range, 0.9–3.6) for BPH and normal prostate, respectively. Logan plots V_T for tumors with GS 3 + 3, 3 + 4, and >3 + 4 were 2.0 (range 1.1–2.3), 2.9 (1.3–5.6), and 3.2 (1.9–8.9), respectively.

Discussion

Recent advances in management of PCa have become possible with improved staging where the role of multimodality imaging is essential. Currently, the majority of men present with localized disease and many can safely undergo active surveillance instead of immediate therapy which potentially

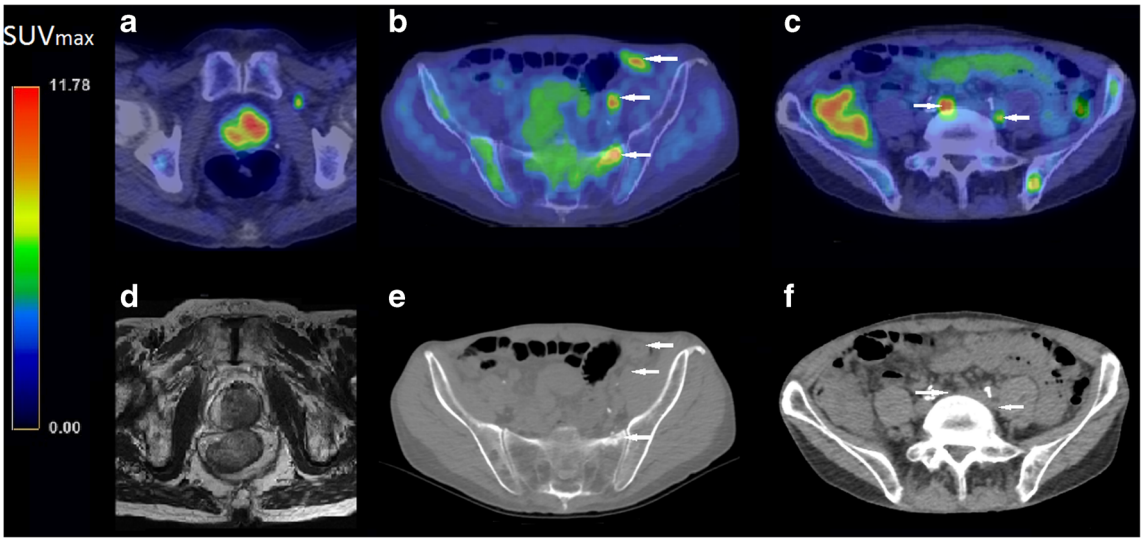

Fig. 1 Patient who presented with PSA of 26 μg/l and GS 5 + 4 PCa on biopsy, showed uptake of ^{18}F-FACBC in the majority of the left peripheral lobe extending from the apex to the base and to the right lobe (A). ^{18}F-FACBC-avid metastases (white arrows) where found in left sacrum and iliac (B) and presacral lymph nodes (C). Corresponding anatomy is shown in T2w MRI (D) and CT (E, F). A is scaled to SUV, with a minimum at 0.00 and maximum at 3.6. B is scaled to SUV, with a minimum at 0.00 and maximum at 3.1. C is scaled to SUV, with a minimum at 0.00 and maximum at 3.1

exposes them to adverse effects and reduced quality of life. Molecular imaging and mpMRI are increasingly available for diagnostic workup and they should be rigorously assessed for their potential to detect intra-prostatic and locally advanced disease, lymph node metastases, and clinical aggressiveness [33]. This led us to undertake the current trial where ^{18}F-FACBC PET/CT, PET/MRI, and mpMRI were studied in treatment-naïve men scheduled for robotic-assisted prostatectomy. Our focus was not only in diagnostic accuracy but quantitative methods which we wanted to relate to pathologic GS, the most important predictor of outcome.

We found similar diagnostic accuracy at the regional level (Table 2) between ^{18}F-FACBC PET/MRI, and mpMRI, which both outperformed ^{18}F-FACBC PET/CT in assessment of intraprostatic disease. ^{18}F-FACBC PET/CT demonstrated a relatively low specificity of 56% because of increased tracer uptake in hyperplastic nodules, a feature typical of tracers depicting various metabolic pathways of PCa. Logan plots did not improve the differentiation of Gleason scores. However, BPH could be reliably discriminated from cancer with MRI using "high" DWI b values, clearly favoring PET/MRI over PET/CT even though PET/MRI was acquired when the ^{18}F-FACBC tumor-to-prostate ratio was decreasing. Ideally, PET/MRI with ^{18}F-FACBC should be performed no later than 10–30 min after injection, based on findings in our own study (Fig. 3) and those of Schuster et al. [11] and Turkbey et al. [13] who imaged the patients with PET/CT only. This time window ensures the best lesion visibility, which is particularly important in the context of definitive radiotherapy involving focally increased doses through simultaneously integrated boost techniques.

^{18}F-FACBC has shown promise in the detection of metastatic lymph nodes among patients with biochemical recurrence after prostatectomy [34]. ^{18}F-FACBC PET/CT is superior to ^{11}C–choline, ^{111}In-capromab pendetide, and CT in restaging of patients after PSA failure, which recently led to US FDA approval of ^{18}F-FACBC (Axumin™) to be used for detection of recurrence of PCa. The largest prospective study of 89 patients presenting with rising PSA found eight patients having true-positive lymph node metastases detected with ^{18}F-FACBC who were false negative with ^{11}C–choline [12]. In that study, ^{18}F-FACBC missed only two patients who presented with true metastatic lymph nodes on ^{11}C–choline PET/CT. Because relapsing PCa is different from that evaluated for primary diagnosis, these findings may not directly reflect those in patients referred to first-line therapy.

Table 2 Diagnostic accuracy at the region level

	Sensitivity	Specificity	Accuracy	AUC (95% CI)
PET/CT	87 (*)	56 ($p < 0.001$)	72	0.72 (0.65–0.80; $p < 0.001$)
PET/MRI	84 ($p = 0.32$)	96 ($p = 0.10$)	90	0.90 (0.86–0.94; *)
mpMRI	77 ($p < 0.01$)	99 (*)	88	0.88 (0.83–0.93; $p = 0.47$)

Sensitivity, specificity, and accuracy values are displayed in %. Two-sided p values are displayed with reference to the combination marked by (*). AUC = area under the receiver operator curve; CI = confidence interval

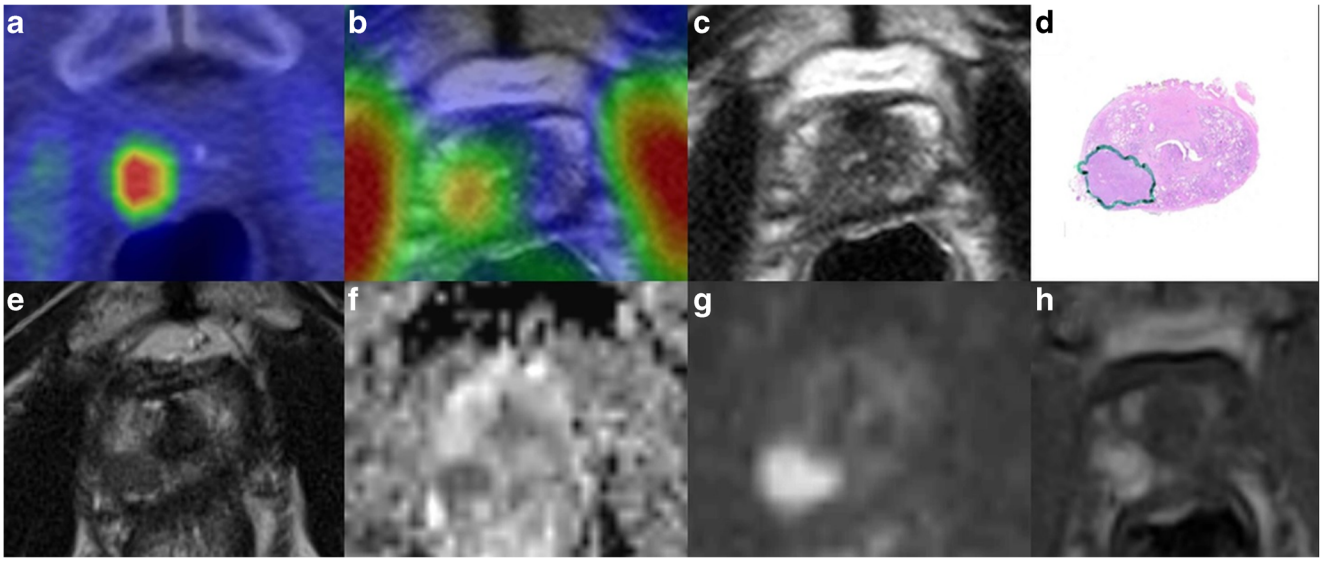

Fig. 2 Right peripheral lesion on ^{18}F-FACBC PET/CT (A) and PET/MRI (B); less conspicuous on T2w PET/MRI (C) of patient no. 3. Whole-mount prostatectomy section (D): tumor classified as pT3a GS 4 + 4. On T2w (E), ADC (F), DWI (b value = 2000 s/mm^2; G), and DCE (H) of mpMRI, the lesion is well demonstrated. Note decreased ^{18}F-FACBC uptake over time for PET/CT vs. PET/MRI. A is scaled to SUV, with a minimum at 0.00 and maximum at 4.7. B is scaled to SUV, with a minimum at 0.00 and maximum at 2.5

Indeed, in assessment of pelvic lymph nodes, the knowledge of performance of ^{18}F-FACBC is slim. The low incidence of lymph node metastases in patients referred to radical prostatectomy contributes to this. For instance, Turkbey et al. found [13] no pelvic metastases in their study of 21 patients. However, they did not report in detail the number of resected lymph nodes, and Schuster et al. [11], in turn, did not report on evaluation of lymph nodes of their 10 patients at all. By contrast, 7 out of 26 patients (27%) in the current study were found to have 22 metastatic lymph nodes where the total number of resected lymph nodes was high at 429. We believe, therefore, that this current study is the first comprehensive evaluation of the potential in assessing pelvic lymph nodes at initial staging. Only one of seven patients, however, had ^{18}F-FACBC-positive metastases, which measured 10–25 mm; the remaining six false-negative patients had metastases <8 mm. DWI resulted in a comparable and low sensitivity for regional metastatic node detection.

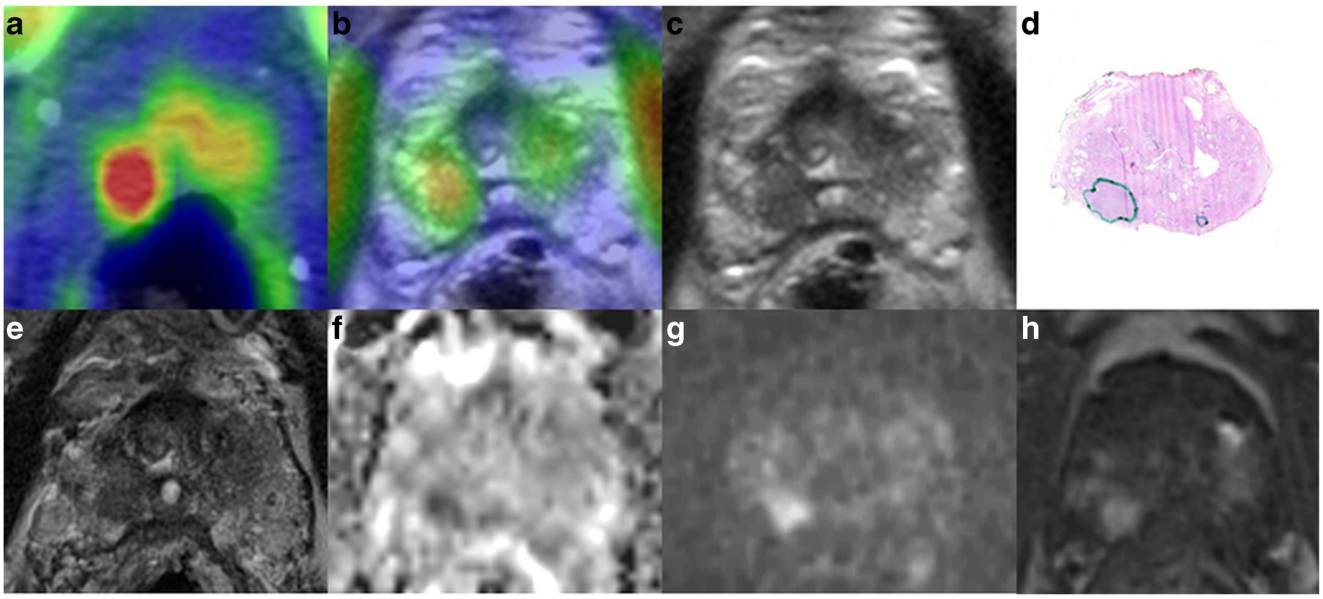

Fig. 3 Right peripheral clearly visible lesion on ^{18}F-FACBC PET/CT (A), PET/MRI (B), and T2w PET/MRI (C) of patient no. 1. Whole-mount prostatectomy section (D): tumor classified as pT2a GS 4 + 3 + 5. A small area of 3 + 3 tumor on the left peripheral zone was not included in the analyses. On T2w (E), ADC (F), DWI (b value = 2000 s/mm^2; G), and DCE (H) of mpMRI, the lesion is well demonstrated. A is scaled to SUV, with a minimum at 0.00 and maximum at 3.9. B is scaled to SUV, with a minimum at 0.00 and maximum at 2.0

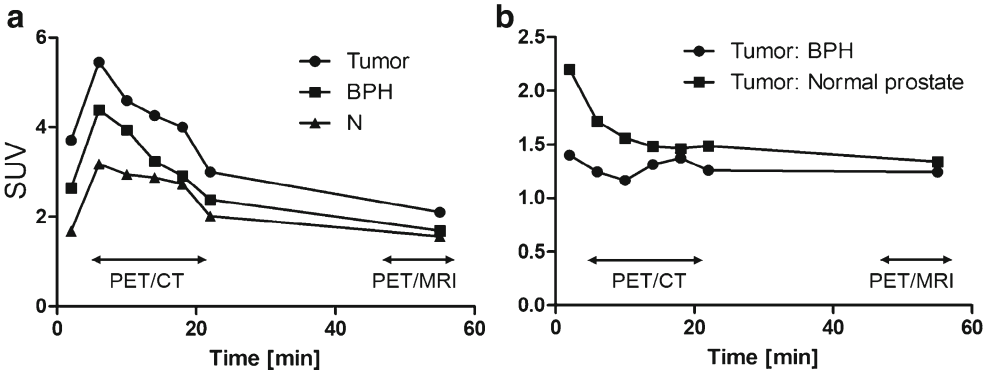

Fig. 4 Median time activity curves for (A) all 41 carcinoma foci, BPH, normal prostate showing rapid increase in SUV followed by a gradual tracer washout. The carcinoma-to-BPH and carcinoma-to-normal prostate ratios (B) were comparable at 12–22 min

The Gleason grading system [35] is the most widely used histopathological marker of PCa aggressiveness [29] and an important component of the treatment decision process [3]. However, systematic TRUS-guided biopsy underestimates true GS based on prostatectomy in up 30% of patients [4]. Development and validation of methods enabling non-invasive estimation of GS could improve PCa risk stratification. V_T derived from Logan analysis showed similar power for GS prediction as SUV_{max} at 12–22 min although the plots did not improve to differentiation of GSs. Dynamic PET data together with the robust measurement of SUV_{max} suggest that high-risk tumors present with high intracellular transport of ^{18}F-FACBC. Transport is dependent on both sodium-independent and sodium-dependent mechanisms where LAT1 and ASCT2 are involved [36, 37]. While low-risk tumors and BPH also present with increased transport of ^{18}F-FACBC, it is, on average, lower, and quantitative evaluation of tracer uptake may thus assist in image-guided biopsies and biologically guided radiotherapy.

After initiation of this study, prostate-specific membrane antigen (PSMA), most commonly labeled with ^{68}Ga has emerged as a tracer of choice for radionuclide imaging of PCa [38]. Based on its high sensitivity to detect biochemical recurrence, the potential of ^{68}Ga-PSMA to image metastatic PCa is already well-established [39], while experience in the primary staging is still more limited [40]. ^{68}Ga-PSMA shows higher uptake in GS > 7 tumors and it is obvious that—like in the case of ^{18}F-FACBC—hybrid imaging with MRI is required for reliable delineation of intraprostatic lesions [38, 41]. Whether ^{68}Ga-PSMA is superior to ^{18}F-FACBC in diagnosis of early PCa requires further study, hopefully in the setting of head-to-head comparison in patients receiving both tracers before prostatectomy. Since the whole-mount prostatectomy sections were obtained at 5-mm (range 4–6 mm) intervals, it is possible that true diameter of some cancer lesions could be under- or overestimated. It is well-known that precise correlation of PCa locations on whole-mount prostatectomy to PET/MRI and mpMRI is relative difficult [42]. Anatomical landmarks, such as the urethra, were used to enable the correlations of whole-mount prostatectomy to PET/MRI and mpMRI images.

In conclusion, primary PCa has increased uptake of ^{18}F-FACBC where lesions with high GS tend to show higher uptake compared to those with GS 3 + 3 and BPH. PET/MRI outperforms PET/CT but did not show higher diagnostic performance than mpMRI performed separately. Furthermore, PET/MRI and mpMRI were not able to detect pelvic lymph node metastases smaller than 8 mm. ^{18}F-FACBC PET/MRI shows promise in characterization of primary PCa especially if focal ablative therapeutic approaches are planned. It is not likely to replace mpMRI in routine clinical practice.

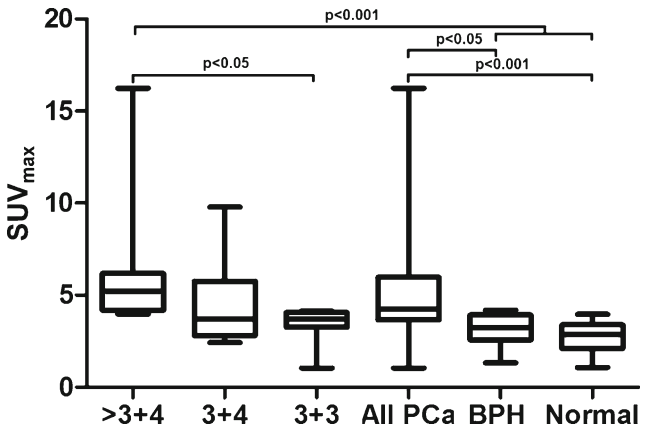

Fig. 5 Median SUV_{max} of ^{18}F-FACBC at 12–22 min of cancerous lesions with GS >3 + 4 (n = 20), GS 3 + 4 (n = 13), GS 3 + 3 (n = 8), all tumors (n = 41), BPH (n = 14), normal prostate (n = 22). Significant differences with corresponding p values are marked

Acknowledgements This work was funded in part by the Finnish Cancer Foundation, Turku University Hospital Research Funds (EVO), TYKS-SAPA research fund, Instrumentarium Research Foundation, Sigrid Jusélius Foundation, Finnish Cancer Society, and the Finnish Cultural Foundation Southwest Finland Regional Fund. We thank the staff of Turku PET Centre and Department of Urology, Turku University Hospital, for practical assistance. We thank Jaakko Liippo (Turku University Hospital, Turku, Finland) for his help in scanning the histological slides and David Gauden (Blue Earth Diagnostics, Oxford, UK) for providing the FastLab cassettes used in radiosynthesis.

Compliance with ethical standards The study was approved by the local ethics committee and each patient gave written informed consent. The study Clinicaltrial.org registration number is NCT02002455.

References

1. Siegel RL, Miller KD, Jemal A. Cancer statistics, 2016. CA Cancer J Clin. 2016;66:7–30.
2. Johnson DC, Reiter RE. Multi-parametric magnetic resonance imaging as a management decision tool. Transl Androl Urol. 2017;6:472–82.
3. Carroll PR, Parsons JK, Andriole G, et al. Prostate cancer early detection, version 2.2015. J Natl Compr Cancer Netw. 2015;13:1534–61.
4. Nepple KG, Wahls TL, Hillis SL, Joudi FN. Gleason score and laterality concordance between prostate biopsy and prostatectomy specimens. Int Braz J Urol. 2009;35:559–64.
5. Jambor I, Borra R, Kemppainen J, et al. Functional imaging of localized prostate cancer aggressiveness using ^{11}C-acetate PET/CT and 1H-MR spectroscopy. J Nucl Med. 2010;51:1676–83.
6. Mena E, Turkbey B, Mani H, et al. 11C-acetate PET/CT in localized prostate cancer: A study with MRI and Histopathologic correlation. J Nucl Med. 2012.
7. Souvatzoglou M, Weirich G, Schwarzenboeck S, et al. The sensitivity of ^{11}C-choline PET/CT to localize prostate cancer depends on the tumor configuration. Clin Cancer Res. 2011;17:3751–9.
8. Umbehr MH, Muntener M, Hany T, Sulser T, Bachmann LM. The role of 11C-choline and 18F-fluorocholine positron emission tomography (PET) and PET/CT in prostate cancer: A systematic review and meta-analysis. Eur Urol. 2013;64:106–17.
9. Kaira K, Oriuchi N, Imai H, et al. L-type amino acid transporter 1 and CD98 expression in primary and metastatic sites of human neoplasms. Cancer Sci. 2008;99:2380–6.
10. Huang C, McConathy J. Radiolabeled amino acids for oncologic imaging. J Nucl Med. 2013;54:1007–10.
11. Schuster DM, Taleghani PA, Nieh PT, et al. Characterization of primary prostate carcinoma by anti-1-amino-2-[(18)F] -fluorocyclobutane-1-carboxylic acid (anti-3-[(18)F] FACBC) uptake. Am J Nucl Med Mol Imaging. 2013;3:85–96.
12. Nanni C, Zanoni L, Pultrone C, et al. F-FACBC (anti1-amino-3-F-fluorocyclobutane-1-carboxylic acid) versus C-choline PET/CT in prostate cancer relapse: results of a prospective trial. Eur J Nucl Med Mol Imaging. 2016.
13. Turkbey B, Mena E, Shih J, et al. Localized prostate cancer detection with 18F FACBC PET/CT: Comparison with MR imaging and histopathologic analysis. Radiology. 2013;270:849–56.
14. Bettinardi V, Presotto L, Rapisarda E, Picchio M, Gianolli L, Gilardi MC. Physical performance of the new hybrid PET/CT Discovery-690. Med Phys. 2011;38:5394–411.
15. Schulz V, Torres-Espallardo I, Renisch S, et al. Automatic, three-segment, MR-based attenuation correction for whole-body PET/MR data. Eur J Nucl Med Mol Imaging. 2011;38:138–52.
16. Jambor I, Pesola M, Merisaari H, et al. Relaxation along fictitious field, diffusion-weighted imaging, and T_2 mapping of prostate cancer: Prediction of cancer aggressiveness. Magn Reson Med. 2016;75:2130–40.
17. Merisaari H, Toivonen J, Pesola M, et al. Diffusion weighted imaging of prostate cancer: Effect of b-value distribution on repeatability and cancer characterization. Magn Reson Imaging Magn Reson Imaging. 2015;33:1212–8.
18. Jambor I, Merisaari H, Taimen P, et al. Evaluation of different mathematical models for diffusion-weighted imaging of normal prostate and prostate cancer using high b-values: A repeatability study. Magn Reson Med. 2015;73:1988–98.
19. Toivonen J, Merisaari H, Pesola M, et al. Mathematical models for diffusion-weighted imaging of prostate cancer using b values up to 2000 s/mm^2: Correlation with Gleason score and repeatability of region of interest analysis. Magn Reson Med. 2015;74:1116–24.
20. Merisaari H, Jambor I. Optimization of b-value distribution for four mathematical models of prostate cancer diffusion-weighted imaging using b values up to 2000 s/mm^2: Simulation and repeatability study. Magn Reson Med. 2015;73:1954–69.
21. Jambor I, Pesola M, Taimen P, et al. Rotating frame relaxation imaging of prostate cancer: Repeatability, cancer detection, and Gleason score prediction. Magn Reson Med. 2016;75:337–44.
22. Jambor I, Kahkonen E, Taimen P, et al. Prebiopsy multiparametric 3T prostate MRI in patients with elevated PSA, normal digital rectal examination, and no previous biopsy. J Magn Reson Imaging. 2015;41:1394–404.
23. Jambor I, Bostrom PJ, Taimen P, et al. Novel biparametric MRI and targeted biopsy improves risk stratification in men with a clinical suspicion of prostate cancer (IMPROD trial). J Magn Reson Imaging. 2017;46:1089–95.
24. Jambor I, Merisaari H, Aronen HJ, et al. Optimization of b-value distribution for biexponential diffusion-weighted MR imaging of normal prostate. J Magn Reson Imaging. 2014;39:1213–22.
25. Kahkonen E, Jambor I, Kemppainen J, et al. In vivo imaging of prostate cancer using [^{68}Ga]-Labeled bombesin analog BAY86–7548. Clin Cancer Res. 2013.
26. Jambor I, Borra R, Kemppainen J, et al. Improved detection of localized prostate cancer using co-registered MRI and ^{11}C-acetate PET/CT. Eur J Radiol. 2012;81:2966–72.
27. Rosenkrantz AB, Kim S, Lim RP, et al. Prostate cancer localization using multiparametric MR imaging: Comparison of prostate imaging reporting and data system (PI-RADS) and Likert scales. Radiology. 2013;269:482–92.
28. Logan J. Graphical analysis of PET data applied to reversible and irreversible tracers. Nucl Med Biol. 2000;27:661–70.
29. Epstein JI, Allsbrook WC Jr, Amin MB, Egevad LL. The 2005 International Society of Urological Pathology (ISUP) consensus conference on Gleason grading of prostatic carcinoma. Am J Surg Pathol. 2005;29:1228–42.
30. Epstein JI. An update of the Gleason grading system. J Urol. 2010;183:433–40.
31. Rutter CM. Bootstrap estimation of diagnostic accuracy with patient-clustered data. Acad Radiol. 2000;7:413–9.
32. Hanley JA, McNeil BJ. A method of comparing the areas under receiver operating characteristic curves derived from the same cases. Radiology. 1983;148:839–43.
33. Wibmer AG, Burger IA, Sala E, Hricak H, Weber WA, Vargas HA. Molecular imaging of prostate cancer. Radiographics. 2016;36:142–59.
34. Ren J, Yuan L, Wen G, Yang J. The value of anti-1-amino-3-18F-fluorocyclobutane-1-carboxylic acid PET/CT in the diagnosis of recurrent prostate carcinoma: A meta-analysis. Acta Radiol. 2016;57:487–93.
35. Gleason DF. Classification of prostatic carcinomas. Cancer Chemother Rep 1. 1966;50:125–8.
36. Sakata T, Ferdous G, Tsuruta T, et al. L-type amino-acid transporter 1 as a novel biomarker for high-grade malignancy in prostate cancer. Pathol Int. 2009;59:7–18.
37. Li R, Younes M, Frolov A, et al. Expression of neutral amino acid transporter ASCT2 in human prostate. Anticancer Res. 2003;23:3413–8.
38. Fendler WP, Eiber M, Beheshti M, et al. ^{68}Ga-PSMA PET/CT: Joint EANM and SNMMI procedure guideline for prostate cancer imaging: Version 1.0. Eur J Nucl Med Mol Imaging. 2017;44:1014–24.
39. Afshar-Oromieh A, Holland-Letz T, Giesel FL, et al. Diagnostic performance of 68Ga-PSMA-11 (HBED-CC) PET/CT in patients

with recurrent prostate cancer: Evaluation in 1007 patients. Eur J Nucl Med Mol Imaging. 2017;44:1258–68.
40. Uprimny C, Kroiss AS, Decristoforo C, et al. ^{68}Ga-PSMA-11 PET/CT in primary staging of prostate cancer: PSA and Gleason score predict the intensity of tracer accumulation in the primary tumour. Eur J Nucl Med Mol Imaging. 2017;44:941–9.
41. Zamboglou C, Wieser G, Hennies S, et al. MRI versus ^{68}Ga-PSMA PET/CT for gross tumour volume delineation in radiation treatment planning of primary prostate cancer. Eur J Nucl Med Mol Imaging. 2016;43:889–97.
42. Meyer C, Ma B, Kunju LP, Davenport M, Piert M. Challenges in accurate registration of 3-D medical imaging and histopathology in primary prostate cancer. Eur J Nucl Med Mol Imaging. 2013;40(Suppl 1):S72–8.